CSIRO PUBLISHING

GPS/CSS Workshop

www.publish.csiro.au/journals/pasa

Publications of the Astronomical Society of Australia, 2003, **20**, 1–5

The Extraordinary Radio Galaxy MRC B1221–423

V. Safouris[1], R. W. Hunstead[1] and O. R. Prouton[2]

[1] School of Physics, University of Sydney, NSW 2006, Australia
vickis@physics.usyd.edu.au
rwh@physics.usyd.edu.au
[2] Department of Astronomy, University of Padova, I-35122 Padova, Italy
prouton@pd.astro.it

Received 2002 July 26, accepted 2002 September 21

Abstract: MRC B1221–423 is a compact steep spectrum (CSS) radio source in the core of a remarkable elliptical galaxy. We examine its environment with long-slit spectra and multicolour images. A high-resolution synthesis image shows the radio source to have a 1″.5 (5.7 kpc) double structure. We use the empirical relationship between jet kinetic power and narrow line luminosity to infer a source age of $\sim 10^5$ yr. The $z = 0.1706$ host galaxy is clearly disturbed, with tidal features and shells providing plausible evidence for a merger with one or more close companions. This evidence leads us to conclude that B1221–423 may be the progenitor of a much larger source, caught at an early stage in its radio evolution. We speculate that it is the interaction and accompanying events which have triggered this young powerful radio source.

Keywords: galaxies: active — galaxies: interactions — galaxies: individual (B1221–423)

1 Introduction

It is widely believed that the onset of AGN activity in galaxies is closely linked to vigorous star formation, possibly in the presence of mergers. The best evidence to date in support of this claim comes from observations of radio-loud objects. Hubble Space Telescope (HST) and ground-based imaging have shown the hosts of $z \sim 1$ 3C radio sources to be old ellipticals with disturbed, knotty rest-frame UV emission that becomes less prominent with increasing radio source size and age (see Longair, Best, & Röttgering 1995; Best, Longair, & Röttgering 1996). MRC B1221–423 is a compact steep spectrum (CSS) radio source which resides well within the envelope of an elliptical galaxy at $z = 0.1706$ (Simpson et al. 1993). The giant host galaxy was optically identified by Bolton, Clarke, & Ekers (1965) and bears the signatures of interaction, including tidal tails and shells. SuperCOSMOS images show a likely merging galaxy to the south to be significantly bluer than the host galaxy. Being relatively nearby compared with the majority of CSS sources, it provides a unique opportunity to study the environment and events associated with the birth of a powerful radio source. In the following sections we present recent observations of the source and its optical counterpart. Throughout the paper we assume $H_0 = 50\,\mathrm{km\,s^{-1}\,Mpc^{-1}}$ and $q_0 = 0.5$; at the redshift of B1221–423, 1″ corresponds to 3.8 kpc.

2 Radio Observations

High-resolution radio images of B1221–423 were obtained with the 6-element Australia Telescope Compact Array (ATCA) in 2001 May. Two frequencies were observed simultaneously (4.8 and 8.6 GHz) with shortest and longest baselines of 450 m and 6 km. Calibration and imaging were performed using routines in the MIRIAD package, with the instrumental gains and bandpass being determined by observations of the nearby phase calibrator B1144–379. The primary flux density calibrator was PKS B1934–638, with assumed flux densities of 5.83 Jy at 4.8 GHz and 2.84 Jy at 8.6 GHz. Dirty images were made with uniform weighting and deconvolved using the Clark CLEAN algorithm (Clark 1980). Phase self-calibration was applied to correct for remaining phase errors due to an unstable atmosphere.

2.1 Radio Images

The resulting images of B1221–423 are shown in Figure 1. Table 1 summarises the imaging details and measured radio properties. At 4.8 GHz, the source appears slightly extended, with a peak surface brightness of 590 mJy beam^{-1}. At 8.6 GHz the source is clearly resolved into a 1″.5 double structure with a projected peak separation of 5.7 kpc; the peak surface brightness is 210 mJy beam^{-1}. By analogy with larger double sources we tentatively refer to these symmetrically located emission peaks as lobes; there is no evidence of a core. The northern lobe is brighter and accounts for 45% of the flux. A third, more diffuse component to the east accounts for 20% of the flux; higher resolution observations are planned.

To test whether the ATCA flux density measurement at 4.8 GHz is affected by missing extended flux, we have compared it with single dish 4.85 GHz measurements from the PMN survey with a 5 arcmin beam (Gregory et al. 1994; Wright et al. 1994) which give a mean flux density of 1124 ± 58 mJy. This value, however, will include a contribution from an unrelated neighbouring source 2.9 arcmin to the northwest (Duncan & Sproats 1992) for which we measure 150 ± 3 mJy at 4.8 GHz. Based on the PMN position, this confusing source falls at the half-power point of the Parkes beam. The corrected PMN flux density of B1221–423 is therefore 1049 ± 58 mJy, consistent with

10.1071/AS02029 1323-3580/03/01001

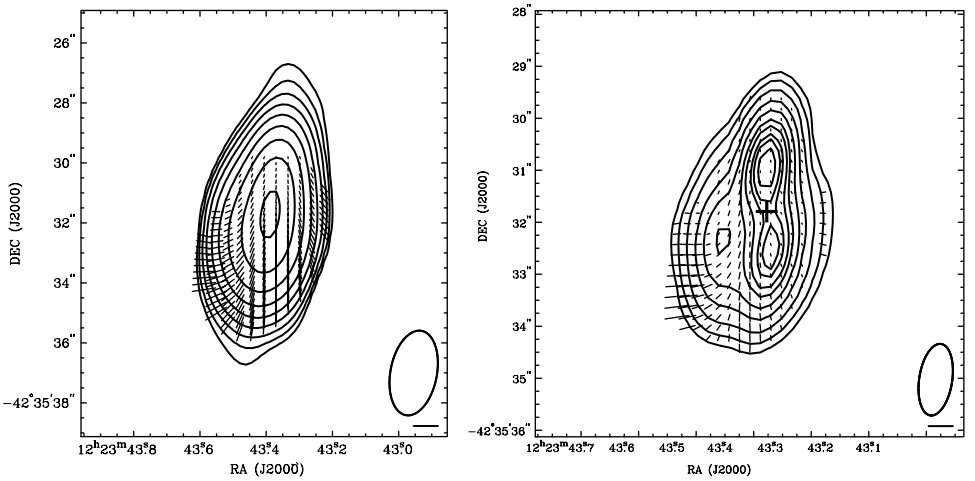

Figure 1 Left: 4.8 GHz total intensity contour map of B1221−423 with contours at 2, 4, 8, 16, 32, 64, 128, 256, 512 mJy beam^{-1}. Right: 8.6 GHz total intensity contour map of B1221−423 with contours at 3.75, 7.5, 15, 30, 50, 75, 100, 130, 150, 180 mJy beam^{-1}; the cross marks the position of the optical nucleus. The restoring beam for each image is shown in the bottom right-hand corner of each panel. The vectors represent the observed E-vectors of the polarised emission with their length proportional to the fractional linear polarisation. The length of the vector corresponding to the maximum polarisation (9% at 4.8 GHz and 35% at 8.6 GHz) is given in the bottom right-hand corner.

Table 1. Imaging details of the radio maps in Figure 1

Frequency (GHz)	Integration time (hr)	Restoring beam	RMS noise (mJy beam^{-1})	Integrated flux density (Jy)	Power (W Hz^{-1})
4.80	7.11	$2''.6 \times 1''.24$ PA = −9.4°	0.160	1.01 ± 0.02	1.8×10^{26}
8.64	7.12	$1''.4 \times 0''.63$ PA = −8.6°	0.145	0.61 ± 0.02	1.1×10^{26}

Note: PA is the position angle of the major axis of the restoring beam, measured north through east.

the ATCA value of 1010 ± 20 mJy, so there is no evidence for extended emission that may have been resolved out in the ATCA observation.

2.2 *Spectrum*

The overall radio spectrum shown in Figure 2 is curved, with a turnover frequency around 100–200 MHz, consistent with the anticorrelation between linear size and turnover frequency for CSS and GPS sources (O'Dea 1998). The two-point spectral index, $\alpha = -0.85$ ($S_\nu \propto \nu^\alpha$), determined from the flux density measurements in Table 1, is slightly steeper than the mean limiting spectral index of -0.73 ± 0.06 found by de Vries, Barthel, & O'Dea (1997) for a sample of 72 GPS sources.

2.3 *Polarimetry*

The observed polarisation vectors are plotted onto the total intensity contour maps in Figure 1. A slight rotation due to the Faraday effect is observed between the two frequencies. The rotation measure (RM) was determined by fitting to individual channel data to remove ambiguities. While the mean rotation measure, RM $= -35$ rad m^{-2}, is

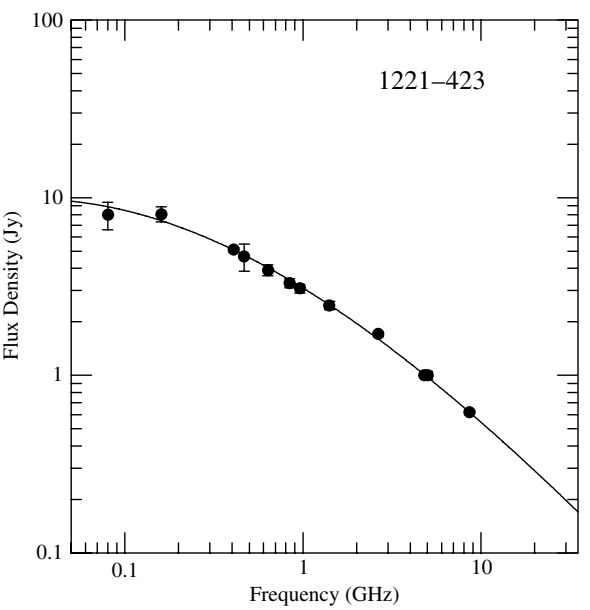

Figure 2 The radio spectrum of B1221−423. Data points are from the literature and from Table 1. A third order polynomial is fitted to the data.

https://doi.org/10.1071/AS02029 Published online by Cambridge University Press

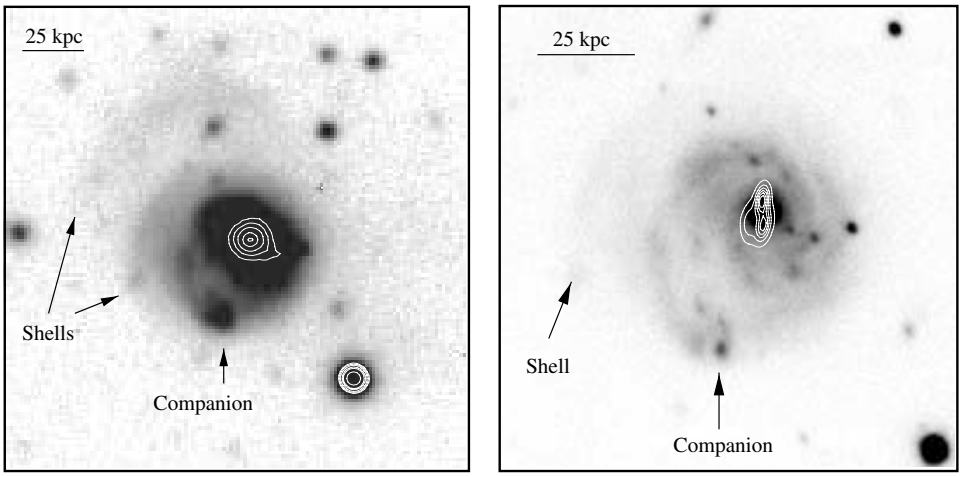

Figure 3 Left: R-band AAT image of the host galaxy in 1″.4 seeing reveals an asymmetric morphology, strongly suggesting an ongoing interaction with a companion galaxy (arrowed); note also the two diffuse shells to the northeast. Optical contours are shown to mark the position of the AGN. Right: R-band NTT image of the host galaxy in 0″.6 seeing shows knotty features and dust lanes closer to the nucleus which mimic the appearance of spiral structure. 8.6 GHz radio contours are overlaid to show the scale of the radio source in relation to the galaxy.

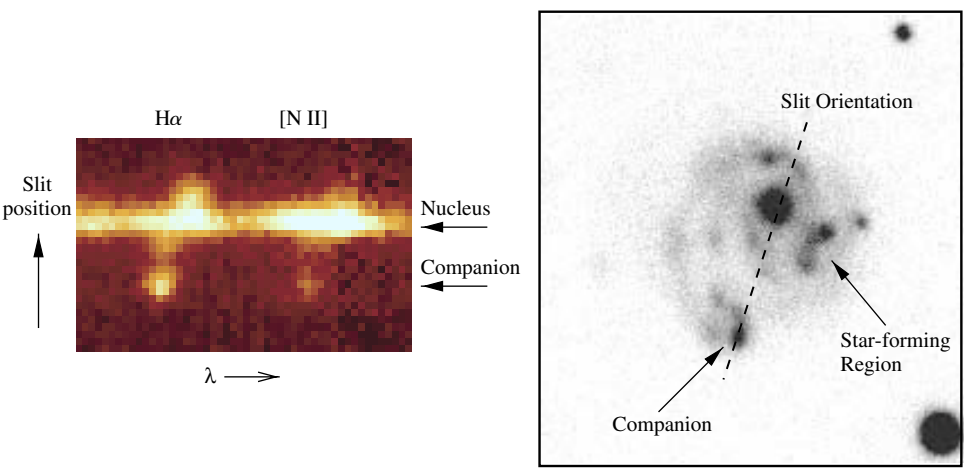

Figure 4 Left: A spectral image taken along an axis joining the host nucleus with the putative companion. Pixel size along the slit is 1″ and the seeing was ∼1.5″. Significant rotation is seen in the Hα and [N II] λ 6583 emission lines. Right: ESO NTT B-band image in 0″.9 seeing showing the orientation of the spectrograph slit.

consistent with Faraday rotation in the foreground screen of our own galaxy (Frick et al. 2001), the RM peaks at $-120\,\mathrm{rad\,m^{-2}}$, indicating some contribution from a magnetoionic screen associated with the host galaxy. From the RMs obtained, we conclude that the true polarisation angles lie mostly within 10° of the observed angles at 8.6 GHz. The projected magnetic field geometry is then inferred to be perpendicular to the jet axis between the lobes, and oriented circumferentially along the outer contours in the lobes, similar to the field patterns seen in much larger sources.

3 Host Galaxy and Source Environment

3.1 Optical Imaging

An R-band image of the host galaxy was obtained in 1993 February with the 3.9 m Anglo–Australian Telescope and Tektronix 1 K × 1 K CCD as part of another program; exposure time was 300 s and seeing was 1″.4. More recently, sub-arcsecond images were obtained in 2001 February with the European Southern Observatory (ESO) New Technology Telescope (NTT) using the Superb Seeing Imager (SUSI2) instrument. The galaxy was observed in Bessell I, R, V, and B filters with exposure times between 400 and 600 s. The data were reduced using the IRAF software package. The AAT and ESO R-band images are shown in Figure 3, and the ESO B-band image is shown in Figure 4. The B-band image includes [O II] which is usually strong in star-forming regions.

The R-band images in Figure 3 show the host galaxy to have a remarkable appearance. Tidal tails, shells, and knotty star-forming regions all suggest that the host is undergoing an interaction with at least one close companion (arrowed) which itself appears disturbed. The

https://doi.org/10.1071/AS02029 Published online by Cambridge University Press

Table 2. Parameters for source age calculation

Frequency (MHz)	Flux density (Jy)	Minimum energy (J m^{-3})	Volume (m^3)	$L_{[O\,II]}$ (W)	Age (yr)
408	5.08	1.8×10^{-10}	2.0×10^{60}	5.1×10^{34}	9.7×10^4

B-band image in Figure 4 (right) is dominated by bright star-forming regions. The southern companion galaxy and the tidal debris extending away from this galaxy are also very blue.

3.2 Spectroscopic Observations

Long-slit spectra were obtained with the Australian National University 2.3 m telescope and double-beam spectrograph at Siding Spring Observatory along three different position angles. The data were reduced using standard techniques in the STARLINK Figaro package. Figure 4 (left) shows a portion of the spectral image taken with the slit aligned along an axis joining the host galaxy to the putative companion. This frame shows significant rotation in the emission lines of Hα and [N II] λ 6583, and also clearly reveals the two galaxies to be at a similar redshift, with $\Delta v = 120 \pm 30$ km s^{-1}. From the spectral data along all three position angles, we determine a maximum gas rotation velocity of 300 km s^{-1} about a projected axis with PA $= 118 \pm 10°$.

Spectra covering 4 arcsec along the slit centred on the host nucleus and companion galaxy were extracted from the spectral image in Figure 4; the slit width was 1″.5. Line analysis was carried out in the IRAF package using the SPLOT routine. The combined spectra showed relatively strong Hα emission over the southern companion galaxy with [N II] λ 6583/Hα $\sim$ 0.3, and relatively strong and broad [N II] emission over the host nucleus with [N II] λ 6583/Hα $\sim$ 1.9. These line ratios provide evidence of active star formation in the southern companion and AGN emission from the host nucleus. Star formation is also evident at other slit positions in Figure 4, notably just north of the active nucleus. A large Balmer decrement was found (Hα/Hβ $\sim$ 8) in the nuclear spectrum, which is indicative of reddening and consistent with other evidence that CSS sources reside in dusty environments (e.g. Baker et al. 2002).

4 Estimating the Source Age

Rawlings & Saunders (1991) find a tight relationship for powerful radio sources between the total jet kinetic power Q and the narrow line luminosity $L_{\rm NLR}$. Their result, $Q \propto L_{\rm NLR}^{0.9\pm0.2}$, extends over four orders of magnitude and fits both compact and extended radio sources. They note that for a total lobe energy U and lobe age τ, the jet power can be written as $Q = U/\tau\eta$, where η is an efficiency parameter allowing for work to be done on the surrounding medium. In their study, the energy U was taken to be the lobe equipartition energy, τ was measured using the spectral ageing method where possible, and η was taken to be 0.5. De Silva (2001) points out that the age of a source can be determined using this relationship if it is assumed that $Q \simeq L_{\rm TOT}$, where $L_{\rm TOT}$ is the total photoionising luminosity. We have estimated the source age using this method with $L_{\rm NLR} = 15 L_{[O\,II]}$ and $L_{\rm NLR} = 0.003 L_{\rm TOT}$, based on the results of Willott et al. (1999). The relevant data for the age calculation with minimum energy conditions are given in Table 2. The $L_{[O\,II]}$ was found using the spectroscopic observations reported in the previous section and the minimum energy density was calculated using the source flux density at 408 MHz (Large et al. 1981) where radiative losses are minimal.

It is worth noting that our age estimate for B1221–423 implies a mean jet propagation velocity of $\sim$0.1 c, consistent with direct measurements of the hot spot advance speeds in compact symmetric objects (e.g. Owsianik, Conway, & Polatidis 1998; Taylor et al. 2000). In contrast, the estimated orbital period of the companion is a few $\times 10^8$ yr, so if there is a causal connection between the interaction and the triggering of the radio emission, it must involve a substantial time delay. This source may prove to be an excellent laboratory for studying such links.

5 Summary and Conclusion

Radio observations of B1221–423 show the source to have a double morphology with a lobe separation of 5.7 kpc. The radio spectrum and polarisation properties are similar to those observed in more extended radio galaxies. The host galaxy is actively forming stars close to the nucleus and is clearly undergoing an interaction with the southern companion galaxy. The spectral data provide evidence of rapid gas rotation, reddening, AGN emission over the host nucleus, and star formation over the companion. Using an empirical relationship between the radio and narrow-line luminosities, we estimate the source age to be $\sim 10^5$ yr. These lines of evidence lead us to conclude that B1221–423 is likely to be the progenitor of a much larger radio galaxy, triggered recently in a dusty environment during the period of interaction and accompanying starburst. The existence of this extraordinary system offers strong circumstantial evidence that interactions and the associated tidal disruption fuel the active nucleus and trigger the radio emission.

Acknowledgments

We thank Helen Johnston for obtaining the 2.3 m spectra, Garret Cotter for assistance with the ATCA observation,

F. Courbin for carrying out the observations at the ESO-NTT, and the two referees for helpful suggestions. The Australia Telescope is funded by the Commonwealth of Australia for operation as a National Facility managed by CSIRO. O.R.P. is supported by the EC RT Network 'POE' under contract HPRN-CT-2000-00138.

References

Baker, J. C., Hunstead, R. W., Athreya, R. M., Barthel, P. D., de Silva, E., Lehnert, M. D. & Saunders, R. D. E. 2002, ApJ, 568, 592
Best, P. N., Longair, M. S., & Röttgering, H. J. A. 1996, MNRAS, 280, L9
Bolton, J. G., Clarke, M. E., & Ekers, R. D. 1965, AuJPh, 18, 627
Clark, B. G. 1980, A&A, 89, 377
De Silva, E. 2001, PhD Thesis, University of Cambridge
de Vries, W. H., Barthel, P. D., & O'Dea, C. P. 1997, A&A, 321, 105
Duncan, R. A., & Sproats, L. N. 1992, PASA, 10, 16
Frick, P., Stepanov, R., Shukurov, A., & Sokoloff, D. 2001, MNRAS, 325, 649
Gregory, P. C., Vavasour, J. D., Scott, W. K. & Condon, J. J. 1994, ApJS, 90, 173
Large, M. I., Mills, B. Y., Little, A. G., Crawford, D. F., & Sutton, J. M. 1981, MNRAS, 194, 693
Longair, M. S., Best, P. N., & Röttgering, H. J. A. 1995, MNRAS, 275, L47
O'Dea, C. P. 1998, PASP, 110, 493
Owsianik, I., Conway, J., & Polatidis, A. 1998, A&A, 336, L37
Rawlings, S., & Saunders, R. 1991, Nature, 349, 138
Simpson, C., Clements, D. L., Rawlings, S., & Ward, M. 1993, MNRAS, 262, 889
Taylor, G. B., Marr, J. M., Pearson, T. J., & Readhead, A. C. S. 2000, ApJ, 541, 112
Willott, C. J., Rawlings, S., Blundell, K. M., & Lacy, M. 1999, MNRAS, 309, 1017
Wright, A. E., Griffith, M. R., Burke, B. F., & Ekers, R. D. 1994, ApJS, 91, 111